13

Structure and properties of layered coatings of alloyed titanium nitride with a dropping metal fraction

© S.V. Ovchinnikov, V.V. Neifeld, A.V. Voronov

Institute of Strength Physics and Materials Science, Siberian Branch, Russian Academy of Sciences,
634055 Tomsk, Russia
e-mail: ovmLMPiN@ispms.ru.

Received August 18, 2023
Revised December 4, 2023
Accepted December 25, 2023

Using electron microscopy, indentation, scratch and tribology techniques, the structural-phase state and mechanic & tribological properties of layered coatings of alloyed titanium nitride were studied depending on the composition of the layers and at different fractions of bronze droplets in the surface layer. The morphological features of growth at various scale levels, the critical concentrations of elements corresponding to structural and phase transformations, and the structural features of coating growth in the droplet region have been established.

Keywords: multicomponent nitride, bronze, laminar structure, electron microscopy, hardness, scratch, tribology.

DOI: 10.21883/0000000000

Introduction

Currently, a promising direction in the synthesis of functional coatings is the production of multi-element multilayer or nanocomposite coatings due to their high mechanical, anti-corrosion and wear-resistant properties [1,2]. One type of such coatings is composite coatings containing inclusions of a soft metal phase in a solid matrix, which simultaneously show high hardness, viscosity [3] and adaptation of tribological properties in a wide temperature range [4–6].

It is known that among such coatings, coatings with inclusions of a copper phase have proven themselves well, which, due to its good ductility, can increase fracture toughness and reduce the coefficient of friction in tribotests [7–10]. For example, in [9] for TiAlN (Ag, Cu) coatings, the best mechanical and antibacterial properties were obtained at a copper concentration of about 20 at.%, in [10] it is shown that the friction coefficient and wear rate decrease with increasing copper concentration, so that at 17 at.% copper, the wear value is $\sim 7.7 \cdot 10^{-14}\,\mathrm{m}^3$, which is approximately an order of magnitude lower than for a steel substrate.

At the same time, it is obvious that the possibilities for increasing properties are determined by the structural-phase state of the coatings in general and the characteristics of the soft phase in particular of its volume fraction, particle sizes, the nature of distribution and conjugation with the matrix, plasticity and strength All these parameters can be controlled to some extent by changing the synthesis conditions or subsequent heat treatment of the coatings. From our point of view, the first possibility can most easily be realized by using arc evaporation or a combined magnetron-arc method for producing coatings while regulating the intensity of the flow for the droplet fraction and its dispersion. With a targeted selection of these parameters and the choice of a system of coating elements, the beneficial results can be obtained. It is noted the fact for example, for TiN-(Ti,Al)N, TiN-(Ti,Mo,Al)N, ZrN-(Zr,Mo,Al)N and CrN-(Cr,Mo,Al)N coating systems, that for the cutting tool the positive effect of droplets on cutting present, which, as the authors believe, is associated with the formation of an intermediate layer of solid lubricant in the area of the droplets [11].

Despite the fact that there are currently a number of works on modeling the patterns of droplets formation in coatings (see references 28−37 in [11]), the diversity and complexity of droplet crystallization factors and their influence on the structure and properties of coatings makes it necessary to conduct comprehensive experimental studies. One of such studies is the present work, in which lamellar coatings of the Ti-Al-Si-Cu-Fe-Mn-N system obtained by a combined magnetron-arc precipitating method were studied. The choice of this system of elements is due to its ability to form lamels with different structures [12,13], including those containing inclusions of the droplet fraction due to the evaporation of the bronze cathode in an arc discharge. The lamellar architecture of the coatings under study is traditional for wear-resistant coatings and is formed by a metal sublayer, load-bearing layers, and a top layer that determines the tribological properties of the coatings. The objectives of the work were to determine the structural-phase state and mechanic & tribological properties of coatings depending on the concentrations of alloying TiN nitride impurities and the volume fraction of the bronze droplet fraction.

1. Experimental procedure

To synthesize the coatings, one were used a modernized, equipped with an arc evaporator and an oil-free pumping system based on an ISP-1000 fore-vacuum spiral pump (Anst Iwata, Japan) and a CryoTorr-250F cryogenic pump

Table 1. Conditions for sputtering of alloyed layers of layered coatings of the Ti-Al-Si-Cu-Fe-Mn-N system

Description of coating, layer	W_{Ti}, W	W_{AlSiCu}, W	I, A	P_{N2}, Pa	U_s, V
1, layer1, TiAlSiCuN	1300	150	–	0.066	−100
1, layer1, TiAlSiCuFeMnN	1300	150	30	0.07	−100
2, layer2, TiAlSiCuN	1300	150	–	0.066	−100
2, layer2, TiAlSiCuFeMnN	1300	150	50	0.07	−100
3, layer3, TiAlSiCuN	1300	400	–	0.066	−100
3, layer3, TiAlSiCuFeMnN	1300	400	30	0.07	−100
4, layer4, TiAlSiCuN	1300	400	–	0.066	−100
4, layer4, TiAlSiCuFeMnN	1300	400	50	0.07	−100

Note. W_T, W_{AlSiCu} — sputtering powers of Ti and AlSiCu targets, respectively; I — arc discharge current of the bronze cathode; P_{N2} — nitrogen pressure; U_s — substrate displacement potential.

(CTI Cryogenics, USA), a Magnetron Coating Sputtering Machine „Kvant" [14]. Lamellar coatings of the Ti-Al-Si-Cu-Fe-Mn-N system were obtained by unbalanced magnetron sputtering of a Ti target (VT 1 alloy−0 (mass.%): Ti — 99.24−99.7, Fe — up to 0.25, C — up to 0.07, Si — up to 0.1, N — up to 0.04, O — up to 0.2, H — up to 0.01), of a composite target $Al_80Si_{10}Cu_{10}$, obtained by pressing copper inserts into an Al-Si alloy disk, and arc evaporation of a bronze cathode (Cu — 85.5, Al – 10, Fe — 3, Mn — 1.5 mass.%) on substrates of steel ShKh 15 and hard alloy T15K6 in a mixture of argon and nitrogen at a total pressure ≈ 0.3 Pa, temperature 300°C and distances between substrates and targets 60−90 mm. Before coating, the substrates were mechanically polished and sequentially washed in acetone, ethyl alcohol and distilled water under ultrasound.

After obtaining a working vacuum $\sim 3 \cdot 10^{-3}$ Pa in the chamber and heating the specimens, sequential deposition of Ti layers was performed for 5 min and TiN (for 16 min) with the substrates in a stationary position relative to the Ti target and its sputtering power of 1300 W, bias potential on the substrates −100 V, total pressure 0.3 Pa and partial nitrogen pressure 0.06 Pa for the TiN lamel. Subsequently, TiAlSi-CuN layers were sputtered for 60 min and TiAlSiCuFeMnN (top layer with bronze drops, sputtering time 45 min) with the rotation of the substrates at a frequency of 10 rpm and simultaneous sputtering and evaporation of components corresponding to the target lamels. In detail, the deposition conditions of alloyed layers of the four studied coatings are presented in Table 1.

The study of the morphology of the growth surface of the coatings and the preparation of foils for electron microscopic analysis of their cross sections was carried out on the Quanta 200-3D microscope, while such analysis itself was carried out on a JEM-2100 transmission microscope, which was also used to determine the elemental composition of various layers by the energy dispersive spectroscopy (EDS). The hardness of the coatings was measured according to the Oliver and Farr method using a tabletop Nanoidenter (TTX NHT2) at different loads (5 and 20 mN) to qualitatively compare the hardness of the layers in 10 prints. Scratch tests were performed on a Revetest RST scratch tester by CSM Instruments with a Rockwell diamond indenter of radius 200 μm at a maximum load of 40 N, scratch length 6 mm and loading speed 30 N/min. The tribological properties of the coatings were determined using a ShKh15 steel ball with a diameter of 6 mm as an opposite element, a load of 1 N, a linear speed of 10 cm/s, a track radius of 5 mm at a humidity of 70% and different lengths of the tribotrack ~ 3 m (to determine the wear rate of the upper layers) and ~ 170 m to assess the long-term change in the friction coefficient. Surface profilometry of the wear tracks was performed using an Alpha-Step IQ contact profilometer (KLA-Tencor, Milpitas, CF, USA) in six transverse sections of each pavement.

2. Results and discussion

2.1. Structure of coating growth

In this section, we will mainly consider the structure of the two upper layers of alloyed multicomponent titanium nitride, since the structure of the α-Ti and TiN nitride layers has been studied quite a long time ago and in detail [16].

As is obvious from the data in Table 1, the main various parameters of coating synthesis are the sputtering power of the AlSiCu alloy target and the current value of the arc evaporator of the bronze cathode. These factors determine the elemental composition and structural-phase transformations during growth, the volume fraction of the droplet fraction, the thickness and properties of coatings.

To assess the influence of the arc evaporator current on the morphology of the growth surface and the fraction of the droplet fraction in the upper TiAlSiCuFeMnN layer, the surface was studied by scanning electron microscopy. Images of the coating growth surface at arc evaporator currents of 30 and 50 A are shown in Fig. 1. As can be seen from these images, the droplets can be round, lenticular, or in the form of stretched strip. These changes in shape reflect sputtering conditions such as rotation of the substrate with an angular velocity of the order of 10 rpm and screening of the central part of the flow from the cathode, which causes some of the droplets to hit the substrate along a tangential trajectory.

The droplet sizes vary in a wide range, which depends on the arc evaporator current and ranges from submicron sizes (from $\sim 0.3\,\mu$m) to tens of μm ($\sim 20\,\mu$m) at an arc current of 50 A, while at an arc current of 30 A droplet size does not exceed 5 μm. Digital image processing (5−6 images

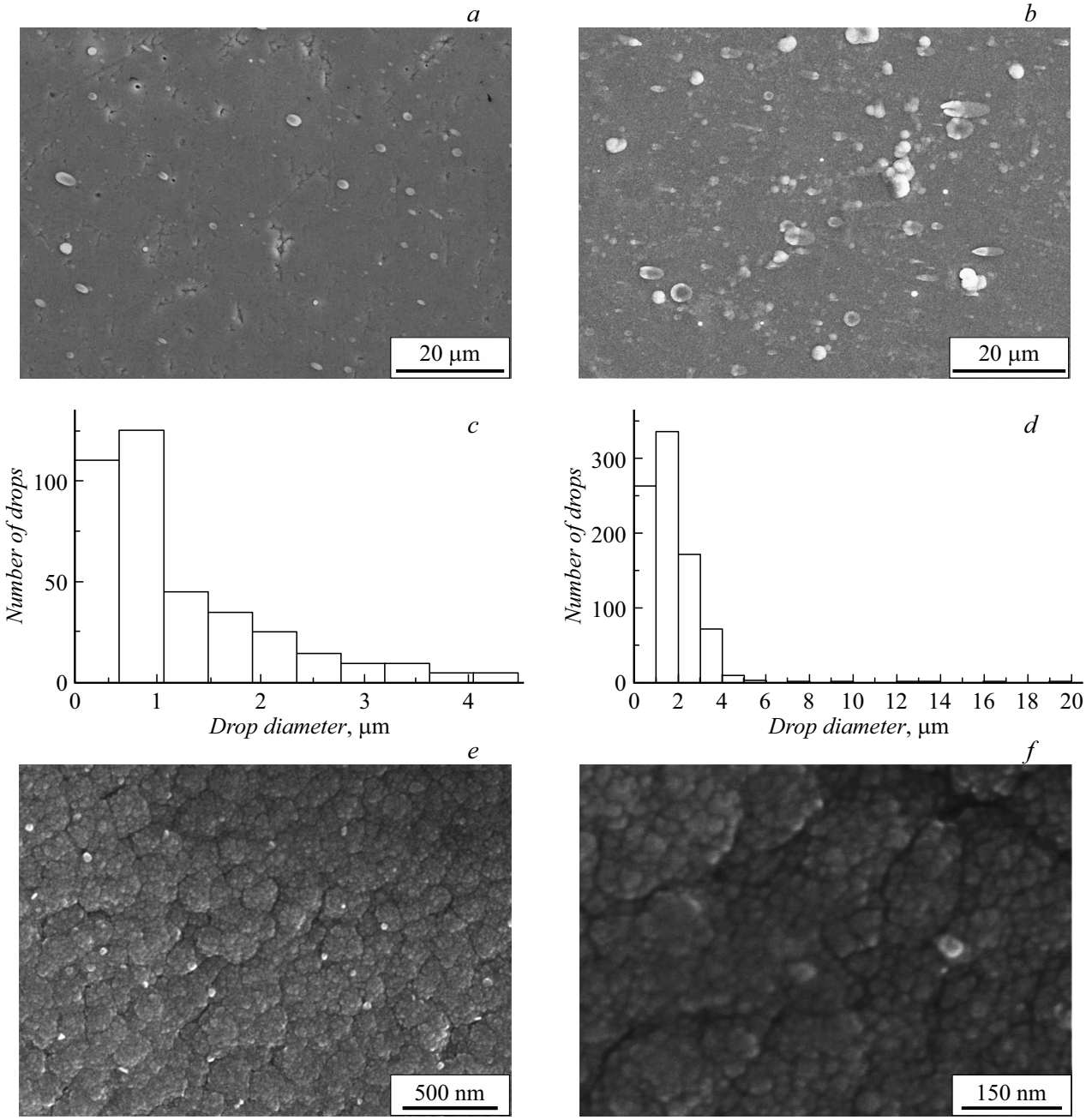

Figure 1. Scanning microscopy of the coating surface, reflecting low (*a*) and high (*b*) density of droplets from the cathode of an arc evaporator, droplet size distribution (*c, d*) and the characteristic cellular morphology of the growth structure at various scale levels (*e,f*), obtained for coatings *1* (*a, c, e, f*) and *4* (*b, d*).

for each type of coating), similar to those presented in Fig. 1, *a, b*, made it possible to perform evaluation calculations with the construction of droplet size distribution (Fig. 1, *c, d*) and estimate their surface and volume fractions in the material of the upper layer. In this case, a spherical shape was taken as an approximation for most droplets, and an ellipsoidal shape for droplets with large non-equiaxial (more than 3). In this approximation, for a coating sputtered at an arc current of 30 A, the volume fraction of droplets is about 1.5%, whereas at an arc current of 50 A, this fraction is approximately equal to 5%. As can be seen from Fig. 1, *c, d*, the largest proportion of droplets are relatively small (no more than $2\,\mu$m) drops, while the proportion of large drops (more than $5\,\mu$m) does not exceed 1%. The given droplet size distributions are qualitatively similar to the results [17] obtained during the deposition of a TiN coating at a multiple higher arc evaporator current (120 A) and are somewhat different from the data [18], where an exponential decrease in the number of droplets depending on their size was found.

The morphology of the growth surface of coatings outside the droplet zone includes, firstly, a relatively large-scale cellular structure, the cell sizes of which can reach $\sim 580-660$ nm (Fig. 1, *e*) with a possible reduction of 2–3 times. Often this structure is not clearly expressed in the form of closed boundaries, but fragmentarily, so that at least one can see open extended boundaries around areas of the specified size. Secondly, large cells are formed by smaller ones with sizes from ~ 10 to 40 nm (Fig. 1,*f*). These last cells, as will be seen from transmission electron microscopy data, are relatively close to the size of the regions of coherent scattering of the crystals of the upper layer, so that in reality they can be the boundaries of crystals (grains). The nature of more extended boundaries is not clear, since according to microscopy data such boundaries are not detected in thin foils. Perhaps these boundaries are a consequence of local topographic contrast associated with heterogeneities in growth at these sizes. In many areas of electron microscopic images of transverse sections of the surface, this local relief can be noted.

The study of the elemental composition of multicomponent nitrides of various coating layers was carried out in cross sections on thin foils using semi-quantitative energy-dispersive X-ray spectral analysis. Let us note the following dependencies. Firstly, with an increase in the arc evaporator current, an increase in the concentrations of arc cathode elements, i.e. Cu, Al, Fe,is quite expected in the upper layer. For example, at a sputtering power of the AlSiCu target of 150 W, an increase in the arc evaporator current from 30 to 50 A leads to an increase in the Cu concentration from 14.4 to 18.9 at.%, Al — from 10.0 to 11.0 at.%, Fe — from 0.5 to 0.8 at.%. To a lesser extent, similar changes are observed for the sputtering power of the marked target of 400 W, but in this case the absolute values of the concentrations are higher. In particular, at an arc evaporator current of 50 A, in this case the concentration of copper reaches 23 at.%, of aluminum reaches about 19 at.%, of iron reaches about 1 at.%. It is obvious that in this case the concentrations of Ti, N and Si decrease, which can reduce both the stability of the FCC lattice and the influence of silicon on the crystal sizes.

Secondly, with an increase in the magnetron sputtering power of the AlSiCu target from 150 to 400 W in the TiAlSiCuN layer, an increase in Al concentrations is observed from ~ 8.7 to 20 at.% and Si from ~ 3.7 to 7.9 at.%. But the concentration of Cu remains virtually unchanged, in the range 3–4 at.%. A similar situation with the copper concentration can be noted for the upper layer at the same arc evaporator current of 30 A. In this case, the copper concentrations (13.5–14.5 at.%) are also approximately the same for sputtering powers of the AlSiCu 150 or 400 W target. Perhaps this phenomenon is due to an increase in secondary (from the coating surface) sputtering of copper during the formation of a nanocrystalline structure, for example, from the region of relatively „loose“ crystal boundaries, where there should be segregation of copper due to its insolubility in titanium nitride.

Thirdly, in all layers of the coating, impurity elements such as carbon and oxygen are found, the average concentrations of which reach 2–3 at.%, and the highest values are approximately twice as high. It is possible that the presence of these elements is due to insufficient degassing of the camera equipment during the heating process before sputtering the coating. At such relatively low concentrations, as is known [19,20], the noted elements should form a continuous series of solid solutions with titanium nitride.

General light-field image of the structure of a lamellar coating with a relatively low level of alloying of its lamels is presented in Fig. 2, *a*. As can be seen from the figure, the total thickness of the coating without taking into account the droplet is about 2.4 μm, while microscopy and profilometry show that drops can rise above the surface by no more than 1 μm. It should be noted that the boundary between the TiN and TiAlSiCuN lamels can be identified by a change in contrast (the contrast line also coincides with the position of a sharp peak on the distribution line of Al and Si concentrations, while the contrast itself is due to a decrease in the effective atomic number when replacing titanium in the metal sub-lattice with lighter ones aluminum and silicon), but the boundaries of columnar grains in many areas pass through it continuously (see arrows *1* in Fig. 2, *b*), i.e. For such a relatively low alloying level of Si (~ 4 at.%), epitaxial growth across the layer interface is observed. The absence of an increase in distortions of the crystal lattice during alloying is also evident from the assessment using the methodology [21] of its bending-torsion, the average value of which for both lamels is close and amounts to $\sim 36^\circ/\mu$m.

At the same time, as can be seen, the upper boundary of the TiAlSiCuN lamel (the boundary between the lamels *4* and *5* in Fig. 2, *a*) has a pronounced relief, which reflects the strengthening of the competitive columnar growth in the alloyed lamel, which can also be noticeable by an increase in grain diameter with increasing coating. This position is also confirmed by the diffraction pattern of the structure of the upper part of the TiAlSiCuN columnar layer (Fig. 2, *c*), which shows bright reflections like $\langle 200 \rangle$ and $\langle 220 \rangle$ for FCC structure, corresponding to the $\{100\}$ texture with the lattice parameter 0.426 ± 0.001 nm. Thus, this lamel is a single-phase multicomponent nitride of the above composition.

The close position of a number of such reflections of the same name $\langle 220 \rangle$ in the diffraction pattern from the region of 170 nm shows an azimuthal misorientation of the corresponding volumes in the range from 4 to 16°, which corresponds to the presence of both high- and low-angle boundaries. Therefore, the dark-field image in Fig. 2, *b*, obtained in one of the group of $\langle 200 \rangle$ reflections, shows the presence of extinction contours in several adjacent grains. Their maximum sizes (some are marked with indicators in Fig. 2, *b*) can reach 60 nm. In addition, grains of other orientations are detected by the presence of reflections of the $\langle 111 \rangle$ type, but their low intensity indicates their small volume fraction and size.

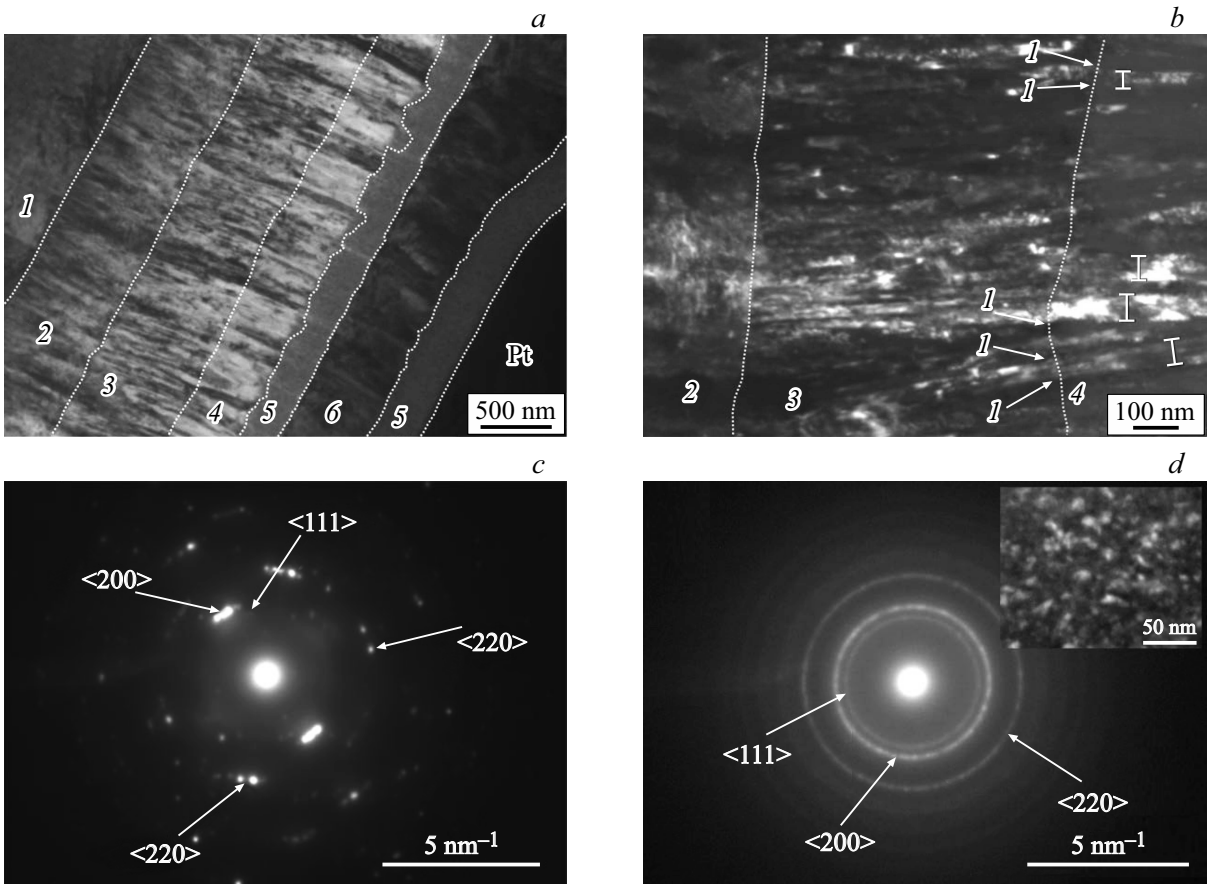

Figure 2. Light- (a) and dark-field (b) overview images and diffraction patterns of the structure of TiAlSiCuN (c) and TiAlSiCuFeMnN (d), obtained at a sputtering power of the AlSiCu target of 150 W and a cathode current of the arc evaporator CuAlFeMn of 30 A; on *1* — substrate, *2* — α-Ti layer, *3* — TiN layer, *4* — TiAlSiCuN layer, *5* — TiAlSiCuFeMnN layer, *6* — dropet of bronze (a, b); c and d show the indices of characteristic reflections from the FCC structure.

The microdiffraction pattern from the top layer of TiAlSiCuAlFeMnN shows characteristic quasi-ring reflections. Calculation of interplanar spacings using them makes it possible to identify an FCC structure with a lattice constant 0.423 ± 0.001 nm (Fig. 2, d), i.e. this layer, like the underlying one, is a single-phase multicomponent nitride, but additional doping led to a decrease in the size of its crystals and lattice constant.

Dark-field images of this structure (see inset in Fig. 2, d) demonstrate its nanocrystalline nature with the size of crystals (coherent scattering regions) in the range 5–20 nm. In this regard, it is necessary to emphasize that in this layer the concentration of such elements as Al and Si, insoluble in Titanium Nitride under equilibrium conditions, is relatively small — $\sim$ 10 and 3.2 at.%, respectively. At such concentrations of these elements, as a rule, nonequilibrium solid solutions with a structure of columnar grains of relatively large (up to 50 nm) diameter [22,23] are formed in alloyed transition metal nitrides. But the concentration of another insoluble impurity, i.e. copper, is $\sim$ 14.5 at.%. Its displacement into the boundary regions of crystals should lead to an increase in crystal lattice distortions (stresses, see, for example, their estimates in [24]) on the growth surface and, thus, interrupt epitaxial growth with the formation of new crystal nucleation centers.

The results of an electron microscopic study of the structure of highly-alloyed (at a sputtering power of the AlSiCu 400 W target) coatings are presented in Fig. 3. The structure of the α -Ti and TiN lamels (lamels *2* and *3* in Fig. 3, a) remains columnar and similar to that previously presented in Fig. 2. However, the next lamel, TiAlSiCuN, due, as noted above, to a higher concentration of alloying elements, primarily silicon, changes the structural state and becomes nanocrystalline, as shown by the dark-field image of its structure in Fig. 3, b . The sizes of most single crystals lie in the range 3–5 nm, but the largest of them can reach 15 nm. However, the phase state of this lamel remains similar to a layer of a similar composition of a less doped coating, i.e. alloying titanium nitride with FCC structure and lattice parameter 0.424 ± 0.001 nm.

In the next upper lamel of TiAlSiCuFeMnN, the crystal structure in terms of crystal sizes becomes homogeneous with their size not exceeding 3 nm. These small crystal sizes lead to a broadening of quasi-ring diffraction reflections on

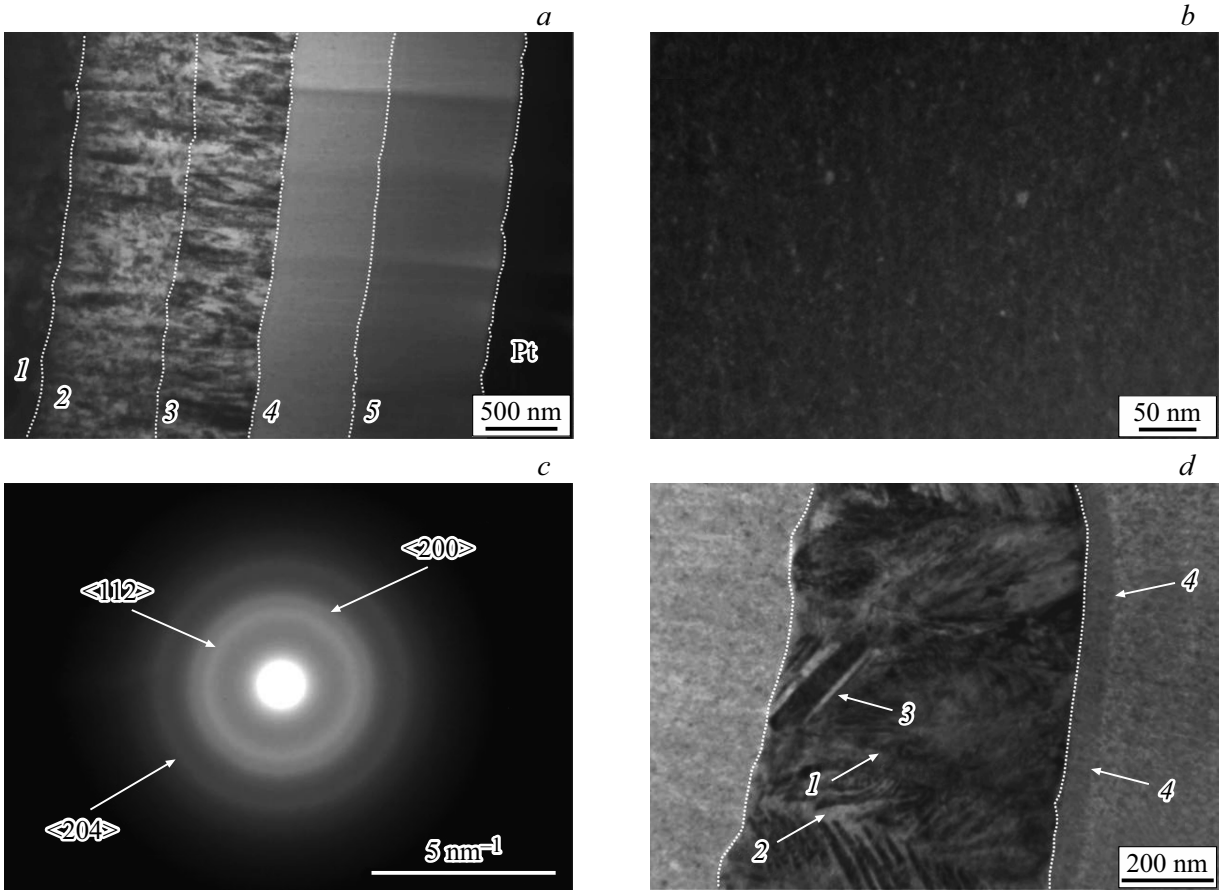

Figure 3. Transmission electron microscopy of the structure of highly doped layered coatings *3* and *4*; *a* — survey-bright-field image; *b* — dark-field image of the nanocrystalline structure of the TiAlSiCuN layer; *c* — microdiffraction pattern of the TiAlSiCuFeMnN layer structure; *d* — bright-field image of a droplet structure from a CuAlFeMn arc cathode. *1* — substrate, *2* — α -Ti layer, *3* — TiN layer, *4* — TiAlSiCuN layer, *5* — layer TiAlSiCuFeMnN (*a, b*); *c* — three most intense reflections of the structure Ti_2 N; *d* — dotted lines — droplet boundaries, arrows: *1* — columnar grain boundary, *2* — dendritic crystal, *3* — lamellar precipitation, *4* — upper boundary of the highly dispersed TiAlSiCuFeMnN layer on the droplet.

Table 2. Values of hardness and Young's modulus of lamellar coatings of the Ti-Al-Si-Cu-Fe-Mn-N system at different indentation loads

Basic conditions of synthesis	Load 5 mN		Load 20 mN	
	Hardness, GPa	Young's Modulus, GPa	Hardness, GPa	Young's Modulus, GPa
$W_{AlSiCu} = 150$ W, $I = 30$ A	10.8	255.13	12.44	293.12
$W_{AlSiCu} = 400$ W, $I = 30$ A	9.35	168.35	12.00	218.34
$W_{AlSiCu} = 150$ W, $I = 50$ A	9.57	233.15	11.2	267.16
$W_{AlSiCu} = 400$ W, $I = 50$ A	10.8	192.23	11.05	213.7

the micro-diffraction of such a structure, as well as to an increased level of diffuse background due to an increase in the volume fraction of crystal boundaries, which can be seen from comparisons of Fig. 3, *c* and Fig. 2, *d*. In addition, calculation of the microdiffraction pattern shows that the ratio of the interplanar spacings corresponding to reflections is different than for an FCC lattice. The elemental composition of this layer is characterized by a high concentration of copper (19−23 at.%), which, as is known [25], helps to reduce the concentration of Nitrogen, which apparently is the reason for the low concentrations of light elements (total for Nitrogen, Oxygen and Carbon up to 30 at.%), outside the stability range of Titanium Nitride [26]. In this regard, the selection of a phase corresponding to the calculated interplanar spacings shows that the most likely candidate for the three strongest reflections marked in Fig. 3, *c* is the Nitride-based phase Ti_2N (space group I41/amd) with parameters $a \approx 0.422 \pm 0.001$ nm, $c \approx 0.922 \pm 0.001$ nm. This is consistent with the data ([27], see section 3.5.4) on the parameters of the tetragonal phase Ti_2N.

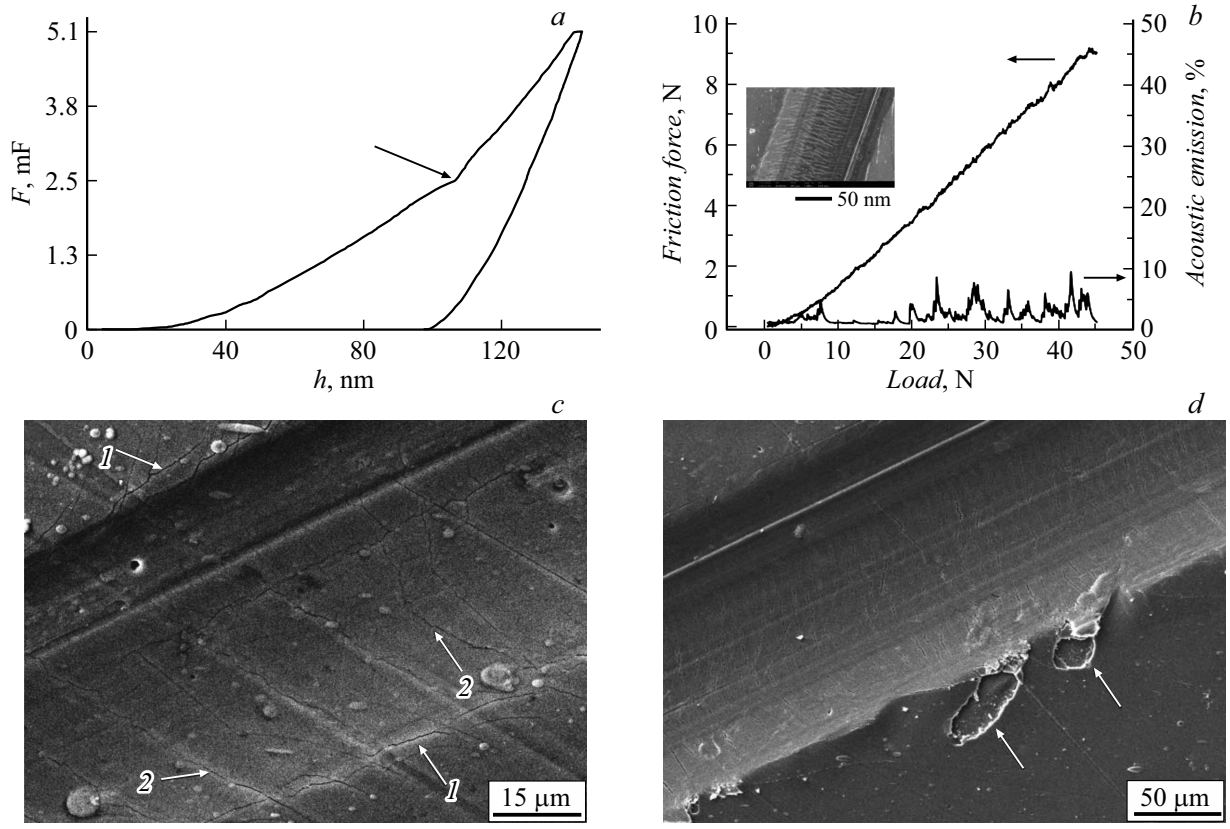

Figure 4. Hardness measurement and scratch testing of coated samples: *a* — loading curve during indentation of a low-alloy coating *1*; dependence of the friction force and the level of acoustic emission on the load (*b*), crack pattern (*c*) and single delaminations (*d*) at a load of about 35 ,N for scratch test of low-alloy coating *2*.

Let us consider the characteristic droplet crystallization structure shown in Fig. 3, *d*, studied for several (in this case, five) droplets. As can be seen, the crystallization conditions (relatively slow heat removal normal to the coating surface) determine the formation of a columnar structure (one of the boundaries of such a structure is marked with an arrow *1* in Fig. 3, *d*) of a solid solution of alloying elements in copper (with dendritic crystals in individual grains — arrow *2* in Fig. 3, *d*) with extended, across the entire width of the columnar grains, lamellar precipitates of the intermetallic compound Cu_9Al_4 (arrow *3* in Fig. 3, *d*). In addition, a feature of the growth of the coating on the droplet is revealed, expressed in the formation of a thin and more dispersed layer on its surface, the boundary of which is marked by arrows *4* in Fig. 3, *d*. Perhaps this modification of the structure is due to a change in the relationship between the rate of formation of crystal nuclei and the value of surface diffusion, which determines the rate of their growth and final dimensions, with increasing coating. With a small thickness of the coating on the droplet, due to the high rate of heat removal through the metal, the density of the seed crystals is relatively high, while subsequently the rate of heat removal through a thicker coating layer slows down, which increases the time it maintains elevated temperatures and, accordingly, the influence of diffusion processes.

2.2. Coating properties

The average values of hardness and Young's modulus of coatings obtained at different indentation loads and instrumental measurement error $\pm 5\%$ are given in Table 2, and a typical loading curve is given in Fig. 4, *a*. In these measurements, loads of 5 and 20 mN were used. The first of them corresponds to an indenter penetration depth of less than 150 nm, i.e. the hardness value is determined predominantly by the properties of the upper layers of TiAlSiCuN and TiAlSiCuAlFeN with a thickness of about $1\,\mu$0m, while with the second load the values of hardness and Young's modulus will be influenced by all lamels of the coating and, to a small extent, by the substrate for coatings obtained at a sputtering power of the AlSiCu target of 150 W. In this connection, it is necessary to note the characteristic point of change in the slope of the indentation curve, indicated by the arrow in Fig. 4, *a*, reflecting an increase in the contribution to the hardness of the TiAlSiCuN layer.

As can be seen from Table 2, with increasing hardness penetration depth, the hardness and Young's modulus increase, i.e. the surface layer is softer, while its lower Young's modulus values are likely due to the high volume fraction of crystal boundaries. A decrease in hardness and Young's modulus is also detected with an increase in the arc

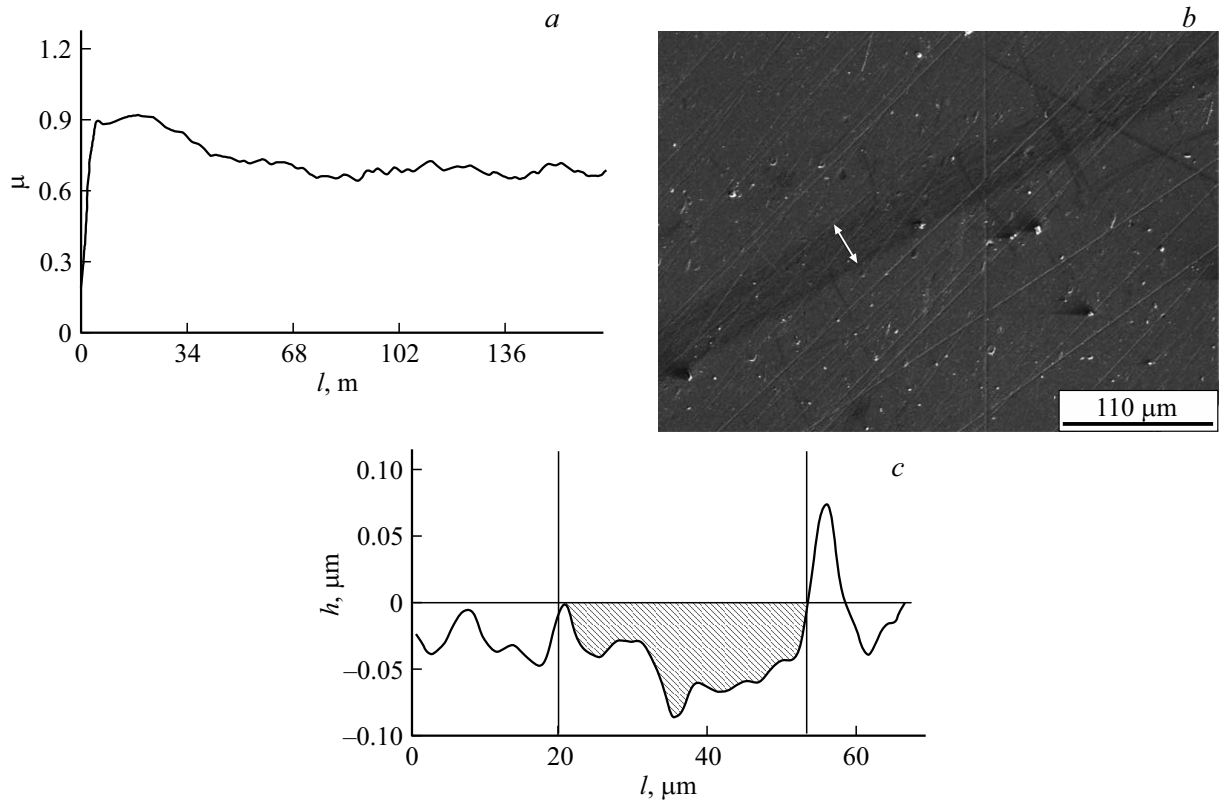

Figure 5. Results of tribological tests of samples of lamellar coatings: dependence of the coefficient of friction on the length of the friction path (*a*), image of the tribo-track (marked with an arrow, *b*) and transverse profile (shaded) of the wear track (*c*) high-alloy coating *3*.

evaporator current, which may be due to an increase in the volume fraction of the droplet fraction and the concentration of copper (the appearance of nanosized copper crystals) in the upper layer in this case. But the opposite trend of changes in the considered characteristics with increasing arc current is shown by coatings with a magnetron sputtering power of the AlSiCu target of 400 W. Currently, this issue requires additional study. It is possible that the reason for this change is an increase in the dispersion of the structure and the volume fraction of crystal boundaries in the upper layer, i.e. essentially its amorphous-crystalline state, as well as the above-mentioned structural transformation of the lattice.

Specific behavior of the friction force and the level of acoustic emission, as well as the SEM image of a scratch (insert) in scratch tests at a load of about 35 N is presented in Fig. 4, *b*. The results of these tests show that the magnitude of the friction force is approximately 20% of the normal load, while the critical load (L_{c1}) for cracking formation in the coating is in the range of2.3−3.05 N and reaches its greatest value at an arc evaporator current of 50Å and sputtering power W_{AlSiCu} 150 W. Probably, such an increase can be associated with a higher fraction of the droplet fraction for this synthesis mode, which promotes the relaxation of stresses applied.

It should be noted that the first cracks parallel to the edge of the scratch are formed at its edge in the area of action of bending and tensile stresses on the surface layer (Fig. 4, *c*, arrows *1*), while cracks along the section of the scratch and perpendicular to its edge (where normal compressive and tangential tensile loads act) are detected at high loads, i.e. in the range 4.5−5 N (Fig. 4, *c*, arrows *2*). As the load increases, the crack density increases and at a load above 20 N the cracks pass through the entire cross section of the scratch, and the distance between them is 5−10 μm (see inset in Fig. 4, *b*). Nevertheless, no delamination of the coatings (with the exception of single delaminations for the coating *2*, Fig. 4, *d*) is detected, i.e. the critical load L_{c2}, which characterizes the adhesive strength for adherence coating to the substrate, exceeds 40−45 N (for different coatings), which is a relatively high value for coatings on steel substrates.

Specific dependences of the change in the friction coefficient on the path length of the counter-instrument, the profilogram of the track section at the initial stages of wear (to determine the wear-resistance of the coating itself, the track length is 3 m) and its image are shown in Fig. 5. As can be seen from Fig. 5, *a*, the friction coefficient almost from the very beginning of the test reaches high values ~ 0.9 maintaining given value up to ~ 25 m length of the test, with a subsequent drop to ~ 0.65 at length ~ 77 m and fluctuations in the range of 0.65−0.73 until the ending of the test (170 m, 4500 rpm). Similar behavior, sometimes with a less pronounced stage of decline in the coefficient

value, is also found for other coatings and in fact does not depend any noticeably on the fraction of the droplet fraction.

Based on profilometry data and computer calculation of the transverse section (S) of the tribo-track (Fig. 5, *b, c*), it is easy to estimate the wear-rate coefficient (k) of the coating from the relationship:

$$k = (2\pi\, r\, S)/(L\, F), \qquad (1)$$

where r and L — radius and length of the tritrack, respectively; F — magnitude of applied load. After substituting tribo-tests and profilometry data into (1), for coatings values k were obtained in the range $(3.4-4.5) \cdot 10^{-14}\,\mathrm{m}^3/(\mathrm{N}\cdot\mathrm{m})$. At the same time, wear resistance is slightly higher for coatings obtained at a maximum arc current of 50 A and a magnetron sputtering power of the AlSiCu target 400 W.

Despite the fact that in this work the tribological properties of the multicomponent TiAlSiCuAlFeN system have been studied, which, as far as the authors know, has not been studied previously, it is of interest to compare the obtained values of tribological characteristics with the data found for similar, similar in composition, coatings of transition metal nitrides alloyed with Cu. Al, Si. As is known (for example, [28]), coatings of the TiAlSiN system have high mechanical properties, but the values of their tribological parameters are low [29,30]. In particular, as established in [30], the value of the coefficient of friction of this coating on steel with a Silicon concentration in it from ~ 4.5 to 15 at.% and is $0.6-0.75$.

A study of the tribological properties of Copper alloyed Nitrides CrN, TiN, MoN [5,7,31–33] shows, firstly, that with a columnar structure of coatings and a high Copper concentration ($\sim 19-21$ at.% and higher), it does not always to carry out tribotests due to rapid wear of the coating [31,32], possibly due to the formation of pores along the boundaries of columnar grains [33]. Secondly, the tribological properties will depend on the ability of the system to form complex double oxides during friction, which reduce the coefficients of friction and wear. For systems CrN-Cu, TiN-Cu [7,33] such oxides are not formed, so the friction coefficient for Copper content is $\sim 20-25$ at.% [7] and ~ 13 at. % [33] has values from $0.6-0.75$ to 0.95, respectively. In other systems with Copper, for example, MoN-Cu [5], such oxides can form, which reduces the friction coefficient severalfold, for example, to ~ 0.22 for the concentration Cu$\sim$ 24 at.% and friction paired work with Al_2O_3 at a load of 3 N. In this case, the wear intensity is $\sim 6 \cdot 10^{-14}\,\mathrm{m}^3/(\mathrm{N}\cdot\mathrm{m})$ and decreases by approximately 7 times when the Copper concentration decreases to$\sim$ 17 at.%. Thus, the tribological characteristics measured in this work are close in their values to those obtained previously for coatings of a similar composition with a high copper concentration.

Conclusion

Based on the research performed, it is necessary to highlight the following patterns of formation of the structure and properties of layered multiphase coatings of the Ti-Al-Si-Cu-Fe-Mn-N system obtained by the combined magnetron-arc method of precipitation. Quantitative dependences of the growth in size and volume fraction of the droplet fraction on the discharge current of the arc evaporator and the absence of direct proportionality between changes in the current strength of the arc evaporator and the noted characteristics of the droplets have been established. It is shown that, in comparison with other alloying elements, the concentration of copper in coatings changes nonlinearly, so that at low densities of plasma flows from an arc evaporator, its value is practically independent of the power of the AlSiCu magnetron source. It has been suggested that secondary sputtering of copper in the nanocrystalline structure is a factor in this phenomenon.

The morphological feature of the growth of the nanocrystalline surface layer in the form of a cellular structure of the sub-microcrystalline and nanoscale levels has been established. It has been shown that the transition to a nanocrystalline state with crystal sizes of $3-20$ nm layers of TiAlSiCuN and TiAlSiCuFeMnN occurs when the Silicon concentration in them reaches a level of $7-8$ at.% (Copper concentration less than 4.5 at.%) or Copper at the level of 14.5 at.% (Silicon concentration less than 3.5 at.%). It was found that at high concentrations of Copper and Silicon in the upper layer of the TiAlSiCuFeMnN coating, a structural transformation of the FCC lattice of alloyed Nitride TiN occurs into a structure that, based on calculations, can be identified as a body-centered tetragonal lattice of alloyed Nitride Ti_2N. Study of the structure of bronze droplets was carried out, which indicates their columnar dendritic crystallization with the release of lamellar intermetallic phases. The formation of a more dispersed layer of coating growth on the surface of the droplets was found.

Measurements of hardness values, strength properties in scratch tests and tribological characteristics of coatings were carried out. For coatings with a low degree of doping of Titanium Nitride with impurity elements (Al, Si, Cu, Fe, Mn) a decrease in the hardness and Young's modulus of the surface layers with increasing proportion of the droplet fraction was determined, whereas with a high degree of doping and in the nanocrystalline state the situation is the opposite. The results of scratch tests show low cohesive strength, while the adhesive strength is high, with a load of peeling of coatings from the substrate of at least 40 N. In tribological tests at the stationary stage of friction, high values of the coefficient of friction of coatings on steel ShKh 15 were established, which actually does not depend on the fraction of the droplet fraction. Based on profilometry of tribotracks, the wear resistance of coatings was calculated, the values of which are in the range $(3.4-4.5) \cdot 10^{-14}\,\mathrm{m}^3/(\mathrm{N}\cdot\mathrm{m})$.

Funding

The research was carried out with State Financial Support from the Fundamental Scientific Research Program of the Institute of Strength Physics and Materials Science of the SB RAS, project № FWRW–2021–0003, using the equipment of the Tomsk Materials Science Center of Tomsk State University.

Conflict of interest

The authors declare that they have no conflict of interest.

References

[1] M.A. Al-Bukhaiti, K.A. Al-hatab, W. Tillmann, F. Hoffmann, T. Sprute. Appl. Surf. Sci., **318**, 180 (2014). DOI: 10.1016/j.apsusc.2014.03.026
[2] J. Lin, J.J. Moore, B. Mishra, M. Pinkas, X. Zhang, W.D. Sproul. Thin Solid Films, **517**, 5798 (2009). DOI: 10.1016/j.tsf.2009.02.136
[3] J. Musil. Surf. Coat. Technol., **125**, 322 (2000). DOI: 10.1016/S0257-8972(99)00586-1
[4] H. Ju, N. Ding, J. Xu, L. Yu, Y. Geng, F. Ahmed. Mater. Chem. Phys., **237**, 121840 (2019). DOI: 10.1016/j.matchemphys.2019.121840
[5] C. Liu, H. Ju, J. Xu, L. Yu, Z. Zhao, Y. Geng, Y. Zhao. Surf. Coat. Technol., **395**, 12581 (2020). DOI: 10.1016/j.surfcoat.2020.125811
[6] H. Ju, N. Ding, J. Xu, L. Yu, I. Asempah, J. Xu, G. Yi, B. Ma. Surf. Coat. Technol., **345**, 132 (2018). DOI: 10.1016/j.surfcoat.2018.04.021
[7] J.C. Ding, T.F. Zhang, Z.X. Wan, H.J. Mei, M.C. Kang, Q.M. Wang, K.H. Kim. Scanning, **2018**, 1 (2018). DOI: 10.1155/2018/6491279
[8] H.J. Mei, R. Wang, X. Zhong, W. Dai, Q.M. Coatings, **8**, 24 (2018). DOI: 10.3390/coatings8010024
[9] H.D. Mejía, A.M. Echavarria, B.G. Gilberto. Thin Solid Films, **687**, 137460 (2019). DOI: 10.1016/j.tsf.2019.137460
[10] D. Hernán Mejía, V.D. Perea, G. Gilberto Bejarano. Surf. Coat. Technol., **381**, 125095 (2020). DOI: 10.1016/j.surfcoat.2019.125095
[11] A. Vereschaka, F. Milovich, N. Andreev, C. Sotova, I. Alexandrov, A. Muranov, M. Mikhailov, A. Tatarkanov. Surf. Coatings Technol., **441**, 128574 (2022). DOI: 10.1016/j.surfcoat.2022.128574
[12] A. Flink, T. Larsson, J. Sjölén, L. Karlsson, L. Hultman. Surf. Coatings Technol., **200**, 1535 (2005). DOI: 10.1016/j.surfcoat.2005.08.096
[13] D. Yu, C. Wang, X. Cheng, F. Zhang. Thin Solid Films, **517**, 4950 (2009). DOI: 10.1016/j.tsf.2009.03.091
[14] V.P. Sergeev, V.P. Yanovsky, Yu.N. Paraev, O.V. Sergeev, D.V. Kozlov, S.A. Zhuravlev. Fizicheskaya mezomekhanika, **22** (7), 2, 333 (2004). (in Russian)
[15] W.C. Oliver, G.M. Pharr. J. Mater. Res., **7** (6), 1564 (1992).
[16] P.H. Mayerhofer, C. Mitterer, L. Hultman, H. Clemens. Prog. Mater. Sci., **51**, 1032 (2006). DOI: 10.1016/j.pmatsci.2006.02.002
[17] V.V. Beregovsky, D.V. Dukhopelnikov, M.K. Marakhtanov, S.A. Schurenkova. Vestnik MGTU im. G.I. Nosova, **4**, 29 (2008). (in Russian)
[18] O.V. Krysina. Avtoref. kand. diss. Tomsk, Institute of High Current Electronics SB RAS, 2016.
[19] L. Karlsson, A. Hörling, M.P. Johansson, L. Hultman, G. Ramanath. Acta Mater., **50**, 5103 (2002). DOI: 10.1016/S1359-6454(02)00365-8
[20] Yu.A. Nechaev, V.M. Kamyshov. Izvestiya AN SSSR. Metally **6**, 50 (1969) (in Russian).
[21] A.D. Korotayev, A.N. Tyumentsev, V.F. Sukhovarov. *Dispersnoye uprochneniye tugoplavkikh metallov* (Nauka, Novosibirsk, 1989) (in Russian)
[22] Y.-C. Kuo, C.-J. Wang, J.-W. Lee. Thin Solid Films, **638**, 220 (2017). DOI: 10.1016/j.tsf.2017.07.058
[23] K.A. Kuptsov, Ph.V. Kiryukhantsev-Korneev, A.N. Sheveiko, D.V. Shtansky. Acta Mater., **83**, 408 (2015). DOI: 10.1016/j.actamat.2014.10.007
[24] S.V. Ovchinnikov, Yu.P. Pinzhin. Rus. Phys. J., **59**, 799 (2016). DOI: 10.1007/s11182-016-0839-z
[25] P. Patsalas, G. Abadias, G.M. Matenoglou, L.E. Koutsokeras, Ch.E. Lekka. Surf. Coat. Technol., **205**, 1324 (2010). DOI: 10.1016/j.surfcoat.2010.09.024
[26] A.I. Gusev. UFN, **170** (1), 3 (2000).. DOI: 10.3367/UFNr.0170.200001a.0003
[27] A.I. Gusev. *Nestekhiometriya, Besporyadok, blizhniy i dal'niy poryadok v tverdom tele* (Fizmatlit, M., 2007)(in Russian)
[28] S. Vepřek, H.-D. Männling, M. Jilek, P. Holubar. Mater. Sci. Eng., A **366**, 202 (2004). DOI: 10.1016/j.msea.2003.08.052
[29] S. Ma, J. Procházka, P. Karvánková, Q. Ma, X. Niu, X. Wang, D. Ma, K. Xu, S. Vepřek. Surf. Coat. Technol., **194**, 143 (2005). DOI: 10.1016/j.surfcoat.2004.05.007
[30] In-Wook Park, Sung Ryong Choi, Ju Huang Suh, Chan-Gyung Park, Kwang Ho Kim. Thin Solid Films, **447**–**448**, 443 (2004). DOI: 10.1016/S0040-6090(03)01122-2
[31] V. Ezirmik, E. Senel, K. Kazmanli, A. Erdemir, M. Ürgen. Surf. Coat. Technol., **202**, 866 (2007). DOI: 10.1016/j.surfcoat.2007.05.049
[32] Jang Ho Shin, Qi Min Wang, Kwang Ho Kim. Mater. Chem. Phys., **130**, 870 (2011). DOI: 10.1016/j.matchemphys.2011.08.002
[33] A. Öztürk, K.V. Ezirmik, K. Kazmanli, M. Ürgen, O.L. Eryilmaz, A. Erdemir. Tribology Intern., **41**, 49 (2008). DOI: 10.1016/j.triboint.2007.04.008

Translated by V.Prokhorov